1   **Genetically encoded intrabody sensors illuminate structural and functional diversity in GPCR-β-**

2   **arrestin complexes**

3   Mithu Baidya[1#], Punita Kumari[1#], Hemlata Dwivedi[1], Eshan Ghosh[1], Badr Sokrat[2], Silvia Sposini[3], Shubhi

4   Pandey[1], Tomek Stepniewski[4], Jana Selent[4], Aylin C. Hanyaloglu[3], Michel Bouvier[2] and Arun K. Shukla[1*]

5   [1]Department of Biological Sciences and Bioengineering, Indian Institute of Technology, Kanpur 208016,

6   India. [2]Institute for Research in Immunology and Cancer (IRIC), Université de Montréal, Montreal,

7   Quebec, H3T 1J4, Canada; Department of Biochemistry and Molecular Medicine, Université de

8   Montréal, Montreal, Quebec, H3T 1J4, Canada. [3]Institute of Reproductive and Developmental Biology,

9   Department of Surgery and Cancer, Hammersmith Campus, Imperial College London, Du Cane Road,

10 London, W12 0NN, UK; [4]Research Programme on Biomedical Informatics (GRIB), Department of

11 Experimental and Health Sciences of Pompeu Fabra University (UPF)-Hospital del Mar Medical Research

12 Institute (IMIM), 08003 Barcelona, Spain.

13 [#]equal contribution; *corresponding author

14 **Keywords:** G protein-coupled receptors (GPCRs), β-arrestins, cellular signaling, synthetic antibody,

15 intrabody, allosteric modulator, biased agonism, trafficking.

16

17

18

19

20

21

22

23

24   **Abstract**

25   Interaction of β-arrestins (βarrs) upon agonist-stimulation is a hallmark of G protein-coupled receptors

26   (GPCRs) resulting in receptor desensitization, endocytosis and signaling. Although overall functional

27   roles of βarrs are typically believed to be conserved across different receptors, emerging data now

28   clearly unveils receptor-specific functional contribution of βarrs. The underlying mechanism however

29   remains mostly speculative and represents a key missing link in our current understanding of GPCR

30   signaling and regulatory paradigms. Here, we develop synthetic intrabody-based conformational sensors

31   that help us visualize the assembly and trafficking of GPCR-βarr1 complexes in cellular context for a

32   broad set of receptors with spatio-temporal resolution. Surprisingly, these conformational sensors

33   reveal a previously unappreciated level of diversity in GPCR-βarr complexes that extends beyond the

34   current framework of affinity-based classification and phosphorylation-code-based interaction patterns.

35   More importantly, this conformational diversity arising from spatial signature of phosphorylation sites

36   manifests directly in the form of distinct functional outcomes, including even opposite contribution of

37   βarrs in signal-transduction for different receptors. Taken together, these findings uncover that despite

38   an overall similar interaction and trafficking patterns; critical structural and functional differences exist

39   in βarr complexes for different GPCRs that define and fine-tune receptor-specific downstream

40   responses.

41

42

43

44

45

46   β-arrestins (βarrs) are multifunctional adaptor proteins, which play a central role in regulation and

47   signaling of G protein-coupled receptors (GPCRs), the largest family of cell surface receptors in our body

48   (1, 2). βarrs are evenly distributed in the cytoplasm under basal condition, and upon agonist-stimulation,

49   they translocate to the plasma membrane to interact with activated and phosphorylated receptors (3).

50   Binding of βarrs to GPCRs at the plasma membrane results in termination of G-protein coupling and

51   desensitization of receptors through a steric hindrance based mechanism (4). Subsequently, βarrs drive

52   receptor clustering in to clathrin-coated pits, via its ability to bind receptor, the β-subunit of the adaptor

53   protein 2 (AP2) and heavy chain of clathrin, resulting in receptor internalization (5). βarrs either

54   dissociate from the receptors and re-localize back in the cytoplasm, or they traffic into endosomal

55   vesicles, in complex with the receptors, a feature associated with kinetics of post-endocytic sorting and

56   βarr-mediated signaling and has led to classification of GPCR/βarr complexes as Class A (transient

57   association, preference for βarr2) and Class B (sustained association, equal associations with βarr1/2)

58   (6). βarrs also play a pivotal role in GPCR signaling by nucleating the components of various MAP kinase

59   cascades such as p38, ERK1/2 and JNK3 (7).

60   As agonist-induced βarr recruitment to GPCRs is a highly conserved phenomenon, it can be used

61   as a surrogate of GPCR activation, and also as a readout of βarr activation resulting in receptor

62   endocytosis and signaling. Currently, a number of approaches are in use to monitor GPCR-βarr

63   recruitment which include FRET/BRET based assays (8), enzyme complementation methods (9) and

64   TANGO assay (10). Each of these methods necessitates a significant engineering and modification of the

65   receptor, the βarr, or both. Here, we develop a set of intrabodies, which can specifically recognize

66   receptor-bound βarr1, and report agonist-induced GPCR-βarr1 interaction and subsequent trafficking

67   with spatio-temporal resolution in cellular context. Surprisingly, these intrabody sensors also reveal a

68   previously unanticipated level of conformational diversity in GPCR-βarr complexes, which goes beyond

69   the current classification of Class A vs. B, and phosphorylation-code-based βarr recruitment, and also

70   functionally linked to distinct patterns of ERK1/2 MAP kinase activation.

71   Agonist-induced receptor activation and phosphorylation are two major driving forces for βarr

72   recruitment and subsequent functional outcomes (11). A phosphorylated peptide corresponding to the

73   carboxyl-terminus of the human vasopressin receptor V2R (referred to as V2Rpp) has been used

74   extensively as a surrogate to induce active βarr conformation in-vitro (12-14). Previously, a set of

75   synthetic antibody fragments (Fabs) have been generated against V2Rpp-bound βarr1 which selectively

76   recognize active conformation of βarr1 as induced by V2Rpp (15). As the first step towards developing

77   these Fabs as potential sensors of βarr1 activation and trafficking, we measured the ability of these Fabs

78   to recognize βarr1 in complex with activated and phosphorylated β2V2R (6). Here, we used a chimeric

79   version of β2AR harboring the carboxyl-terminus of the V2R, referred to as β2V2R which interacts with

80   βarrs strongly. We observed that these Fabs were selectively able to interact with β2V2R-βarr1 complex

81   that is formed upon agonist-stimulation of cells (Figure S1A-D).

82   A key step in developing these Fabs into cellular sensors of βarr1 activation and trafficking is to

83   express them in a functional form in the cytoplasm as intrabodies. We therefore converted the selected

84   Fabs into ScFvs (single chain variable fragments) by connecting the variable domains of their heavy and

85   light chains through a previously optimized flexible linker (16), and then expressed them in mammalian

86   cells as intrabodies either with a carboxyl-terminal HA tag or YFP fusion (Figure 1A-C and Figure S2A).

87   We observed robust expression of two of these intrabodies namely Intrabody30 (Ib30) and intrabody4

88   (Ib4) in HEK-293 cells while others displayed relatively weaker expression (Figure 1B-C and Figure S2A).

89   We also observed a significant level of nuclear localization of the intrabodies but the underlying reasons

90   for this is currently not apparent to us. Interestingly, previous studies using intrabodies against β2AR

91   such as nanobody 80 also reported a similar nuclear localization of fluorescently-tagged intrabodies (2) .

4

92   We then tested whether intrabodies maintain their ability to selectively recognize receptor-

93   bound βarr1 in cellular context. For this, we first chose β2V2R because not only it forms a complex with

94   βarr1 that is well-established to be recognized by Fab30 (*14, 16*), but also a set of ligands with broad

95   efficacy profiles are available to allow in-depth characterization of intrabody sensors. We co-expressed

96   β2V2R, βarr1 and selected intrabodies in HEK-293 cells, stimulated the cells with either an agonist or an

97   inverse-agonist, and then immunoprecipitated intrabodies using carboxyl-terminal HA tag. We observed

98   that both intrabodies i.e. Ib30 and Ib4 robustly recognized receptor-bound βarr1 exclusively upon

99   agonist-stimulation (Figure 1D-E). Moreover, we also observed that the level of recognition of the

100   receptor-βarr1 complexes by Ib30 mirrors the efficacy of the ligands (Figure 1F-G), which in turn further

101   confirms the suitability of these intrabodies as a reliable sensor of βarr1 recruitment to the receptor and

102   its activation.

103   We then co-expressed the β2V2R, βarr1-mCherry and YFP-tagged intrabodies in HEK-293 cells to

104   monitor their trafficking patterns by confocal microscopy (Figure 1H and Figure S2B-D). As expected for

105   β2V2R which behaves like a class B GPCR, we observed plasma membrane translocation of cytosolic

106   βarr1 within a few minutes of agonist-stimulation, and interestingly, YFP-tagged intrabodies co-recruited

107   with βarr1 to the plasma membrane and colocalized (Figure 1H, middle panel and Figure S2B). After

108   prolonged agonist-exposure, βarr1 trafficked to the endosomal vesicles and once again, intrabodies

109   exhibited co-localization with βarr1 (Figure 1H, lower panel and Figure S2B). Line-scan analysis further

110   confirmed colocalization of intrabody sensors with βarr1 (Figure S2C-D). These observations taken

111   together elucidate the ability of these intrabodies to faithfully report the trafficking pattern of βarr1

112   upon agonist-stimulation.

113   As these intrabodies were originally generated against V2Rpp-bound βarr1 conformation, we

114   envisioned that they might be able to report βarr1 recruitment and trafficking for other chimeric GPCRs

115   harboring the V2R-carboxyl-terminus. We therefore generated a set of chimeric GPCRs with V2R-

116   carboxyl-terminus and measured the ability of Ib30 to recognize receptor-βarr1 complex by

117   coimmunoprecipitation and trafficking of βarr1 by confocal microscopy (Figure 2A-X and supplementary

118   Figures S3-S9). We observed that similar to β2V2R, Ib30 sensor robustly recognized receptor-βarr1

119   complexes for this broad set of chimeric receptors and also reported trafficking pattern of βarr1 with

120   spatio-temporal resolution (Figure 2A-X and supplementary Figures S3-S9). These data establish that

121   Ib30-YFP can be used as a generic tool to visualize agonist-induced βarr1 recruitment to the receptor

122   and its subsequent trafficking in cellular context.

123   βarrs are capable of recognizing majority of GPCRs despite poorly conserved primary sequence

124   of these receptors via agonist-induced receptor phosphorylation that drives βarr recruitment and

125   activation. Therefore, we hypothesized that the intrabodies described here may recognize βarr1, and act

126   as a sensor, for native GPCRs as well, considering that structural determinants for βarr1 recruitment and

127   activation are likely to be conserved across the receptors. Accordingly, we next set out to test the

128   intrabody30 on a broad set of native GPCRs using a combination of coimmunoprecipitation and confocal

129   microscopy (Figure 3, Figure 4A-B, and Figure S10-12). We selected these receptors to encompass not

130   only representatives of Class A and B (in terms of their interaction patterns with βarrs) but also a broad

131   pattern of receptor phosphorylation codes proposed recently (17) (Figure 3A and Figure 4A). We started

132   with V2R first and measured the ability of these intrabodies to recognize its complex with βarr1. We

133   observed a pattern very similar to that of β2V2R in both, the the ability of Ib30 and Ib4 to form a

134   complex with βarr1 via co-immunoprecipitation and co-traffic to the plasma and endomembrane

135   compartments following receptor activation-(Figure 3B, 3D and Figure S10). V2R is classified as a class B

136   GPCR based on its stable βarr recruitment pattern and co-internalization in complex with βarrs to

137   endosomal vesicles. Expectedly, we observed a robust co-localization of V2R in endosomal vesicles with

138 βarr1 and Ib30 which further confirms the ability of intrabodies to recognize receptor-βarr1 complexes

139 and follow their endosomal translocation (Figure 3B and S13).

140 Our results mentioned above for V2R strongly underscore the ability of intrabody sensors to

141 report βarr1 recruitment and trafficking without any modification of the receptor or βarr1. As we had

142 set-out to develop these intrabodies as specific sensors of βarr1 recruitment and trafficking, it is

143 important that they do not exhibit any significant effect on heterotrimeric G-protein coupling. To

144 confirm this, we measured agonist-induced cAMP response for V2R in presence of these intrabodies and

145 observed that intrabodies did not significantly alter the kinetics or maximal cAMP response (Figure

146 S14A-B). In addition, we also measured the effect of intrabodies on overall recruitment of βarr1 to the

147 receptor, agonist-induced receptor endocytosis, and activation of ERK1/2 MAP kinases. As presented in

148 Figure S15A-B, intrabodies slightly inhibited the recruitment of βarr1 to the plasma membrane but

149 enhanced agonist-induced receptor endocytosis, as measured by BRET assays. They however did not

150 significantly influence the kinetics of βarr1 localization in early endosomes (Figure 13B) or agonist-

151 induced ERK1/2 phosphorylation (Figure S15C-F). Taken together, these data establish the suitability of

152 Ib30 and Ib4 as a reliable sensor of receptor-βarr1 interaction, and subsequent trafficking of βarr1 in

153 cellular context for native V2R.

154 We next tested the ability of Ib30 sensor to report the recruitment and trafficking of βarr1 for a

155 broad set of native class B GPCRs including the complement C5a receptor (C5aR1), the atypical

156 chemokine receptor 2 (ACKR2), the muscarinic M2 receptor (M2R), the vasopressin receptor sub-type 1b

157 (V1bR), the angiotensin II type 1s receptor (AT1aR) and the bradykinin B2 receptor (B2R) (Figure 3B and

158 Figure S11). These receptors not only couple to different sub-types of G-proteins but also harbor a

159 diverse range of phosphorylation-codes in their carboxyl-terminus and the 3rd intracellular loops (Figure

160 3A). We observed that Ib30 sensor worked efficiently for a number of these receptors including C5aR1,

161   ACKR2, V1BR and M2R (Figure 3B and 3D). Interestingly however, it failed to recognize βarr1 upon

162   stimulation of several others such as the AT1aR and B2R (Figure 3C) although these receptors exhibited

163   significant level of βarr1 recruitment.

164   We also tested the ability of Ib30 sensor to report the recruitment and trafficking of βarr1 for a

165   broad set of native class A GPCRs including the muscarinic M5 receptor (M5R), the muscarinic M3

166   receptor (M3R), the β2-adrenergic receptor (β2AR), the dopamine D2 receptor (D2R) and the α2-

167   adrenergic receptor (α2BR) (Figure 4A-B and Figure S12). These receptors also couple to different sub-

168   types of G-proteins and harbor a diverse range of phosphorylation-codes in their carboxyl-terminus and

169   the 3rd intracellular loops (Figure 4A). Similar to class B GPCRs mentioned above, we observed that Ib30

170   sensor robustly recognizes βarr1 for the muscarinic M5 receptor (M5R) and the muscarinic M3 receptor

171   (M3R) but not for others. Taken together, the Ib30 reactivity pattern suggests that the conformation of

172   βarr1 in complex with various receptors can be significantly different from each other despite

173   comparable patterns of overall gross βarr1 recruitment. We note here that M3R and M5R did not induce

174   any significant endosomal localization of βarr1 even after prolonged agonist-stimulation as expected for

175   class A GPCRs.

176   An interesting observation here is the ability of Ib30 sensor to robustly recognize βarr1 upon

177   stimulation of muscarinic receptors namely M2R, M3R and M5R. This is striking because these

178   receptors, unlike V2R, possess relatively large 3rd intracellular loop and very short carboxyl-terminus

179   (Figure 4C). More importantly, they harbor the full phospho-codes exclusively in their 3rd intracellular

180   loops. The reactivity pattern of Ib30 suggests that these receptors, despite having phosphates in distinct

181   receptor domains, are able to induce a conformation in βarr1 that allows recognition by Ib30. As

182   mentioned earlier, the crystal structure of V2Rpp-βarr1 complex reveals the docking of V2Rpp on the N-

183   domain of βarr1. Thus, it is tempting to speculate that these receptors may also be able to engage an

8

184   identical, or at least similar, interface on βarr1 through their 3rd intracellular loops harboring the

185   phosphorylation sites. In order to test this hypothesis and further corroborate our findings, we

186   measured the interaction of M2R with βarr1 in presence and absence of V2Rpp. As presented in Figure

187   4C, pre-incubation of V2Rpp with βarr1 robustly inhibits the interaction between M2R and βarr1, and

188   therefore, suggest that M2R engages βarr1 through the N-domain interface similar to that engaged by

189   V2Rpp. This is particularly intriguing as the first step in GPCR-βarr interaction is typically considered to

190   involve the phosphorylated carboxyl-terminus followed by the core interaction involving the

191   intracellular loops of the receptors. Considering the short carboxyl-terminus of muscarinic receptors

192   typically devoid of any phosphorylation codes, coupled with much larger, phosphorylation code

193   containing 3rd intracellular loop (ICL3), it is tempting to speculate a distinct mode of receptor-βarr

194   interaction compared to other GPCRs. In fact, a recent study on M1R using optical reporters suggests

195   two distinct conformations of receptor-bound βarrs, which are also distinct from biphasic interaction

196   observed for other prototypical GPCRs (*18*). Furthermore, it also raises the possibility that other

197   receptors harboring short C-terminus but long ICL3 such as the dopamine D2 receptor and α-adrenergic

198   receptors, may also display distinct binding conformations compared to other prototypical GPCRs.

199   The findings described up to this point have two important implications. First, they establish the

200   utility of the intrabody sensors described here as a robust tool to visualize agonist-induced βarr1

201   recruitment and trafficking for a number of GPCRs. Second, they imply that different receptors induce

202   distinct conformations in βarr1 even if they exhibit a similar pattern of gross-recruitment (e.g. V2R vs.

203   B2R) and harbor a similar phospho-code signature in their carboxyl-terminus and 3rd intracellular loops

204   (Figure S16). This prompted us to ask if these distinct conformations of βarr1 for different receptors

205   might have different functional consequences. In order to probe this possibility, we measured agonist-

206   induced ERK1/2 MAP kinase activation for selected receptors and the role of βarr1 in this process (Figure

207   5A-B and Figure S17-18). As discussed earlier, one of the key contributions of βarrs in GPCR signaling is

208   their ability to mediate agonist-induced phosphorylation and activation of ERK1/2 MAP kinases (7). We

209   observed that knockdown of βarr1 yielded a significant reduction in ERK1/2 phosphorylation for V2R

210   while it augmented the levels of ERK1/2 phosphorylation activated by GPCRs that did not recruit the

211   arrestin intrabodies such as B2R and AT1aR (Figure 5A-B and Figure S17-18). These striking differences in

212   the functional contribution of βarr1 in agonist-induced ERK1/2 activation suggests a potential link

213   between the receptor-bound βarr1 conformation and different functional outcomes, and also provide a

214   potential structural mechanism for how receptor-specific βarr conformations encode functional

215   differences. An important implication of this data is that βarr1 conformation upon stimulation of B2R is

216   competent to drive endocytosis but suppressive towards ERK1/2 phosphorylation.

217   As mentioned above, both V2R and B2R belong to class B GPCRs, in terms of βarr recruitment

218   patterns, and they each harbor two full phosphorylation codes in their carboxyl-terminus. This suggests

219   that distinct patterns of Ib30 reactivity and ERK1/2 phosphorylation arise elsewhere. A close comparison

220   of the carboxyl-terminus of these two receptors revealed a difference in the spatial distribution of the

221   phosphorylation sites (Figure 5C). This prompted us to generate a set of B2R mutants to resemble the

222   pattern of phosphorylation in V2R (Figure S19A). These mutants exhibited comparable surface

223   expression levels similar to wild-type B2R (Figure S19B). Out of these mutants, we did not observe any

224   detectable reactivity of Ib30 for $B2R^{\Delta G368}$ and $B2R^{I374S}$ although they robustly recruited βarr1 (Figure

225   S20A-B). Interestingly however, we found robust reactivity of Ib30 in case of $B2R^{\Delta G368+L374T}$ and $B2R^{L374T}$

226   (Figure 5C, Figure S19B). These findings reveal that spatial signature of receptor phosphorylation sites

227   play a detrimental role in ensuing βarr1 conformation recognizable by Ib30. Even more strikingly, we

228   discover that βarr1 plays a positive role in phosphorylation of ERK1/2 for the $B2R^{\Delta G368+L374T}$ and $B2R^{L374}$ as

229   the lack of βarr1 results in a substantial reduction (Figure 5D and Figure S19C-D). The pattern of ERK1/2

230   phosphorylation for $B2R^{\Delta G368+L374T}$ and $B2R^{L374}$ is similar to that of V2R, and it is in stark contrast with the

231   wild-type B2R, thereby linking the βarr1 conformation, as read by Ib30, with subsequent functional

10

232   outcome. These striking observations indicate that βarr1 adopts a conformation upon stimulation of

233   B2R$^{\Delta G368+L374T}$ and B2R^{L374} that is capable of supporting both, endocytosis and ERK1/2 phosphorylation,

234   unlike the wild-type B2R.

235   In order to gain structural insights into the recognition of B2R mutants by intrabody30 sensor,

236   we employed molecular dynamics simulation approach using the previously determined crystal

237   structure of βarr1 in presence of V$_2$Rpp. We carried out MD simulations with V2Rpp, B2Rpp and the

238   mutant version of B2Rpp (derived from B2R^{L374T}) (Figure S21A). We observed that in the B2Rpp mutant

239   as well as V2Rpp, L360pT together with pT359 interacts with K294 in the lariat loop via strong

240   electrostatic interactions (Figure S21B, blue bar plots). Such bifurcated contacts seem to stabilize the

241   lariat loop preferential in conformational states belonging to cluster 1 (Figure S21C, blue lines in

242   structure and blue bar plots). Cluster 1 overall resembles the conformation of the crystallized lariat loop

243   in complex with Fab30 (pdb 4JQI) with an average rmsd of 1.9 Å. Such bifurcated linkage of the lariat

244   loop to the phosphorylated receptor C-tail is lost in the B2Rpp WT as the non-polar L360 cannot

245   establish an interaction with K294 (Figure S21B, red bar plot). As a consequence, the loop conformation

246   is shifted downwards favoring cluster 2 (Figure S21C), red lines in structure and red bar plot). This yields

247   a dramatic increase of average rmsd to 4.6 Å with respect to the crystallized lariat loop. It is likely that

248   such conformational change of the lariat loop in the Fab30 binding interface contributes to a decreased

249   Fab30 binding. Overall, MD data together with site directed mutagenesis suggest that the lariat loop in

250   βarr1 may provide an important site for driving conformational differences in different GPCR-βarr1

251   complexes, at least as measured by intrabody30 reactivity.

252   Taken together, we develop intrabody-based sensors, which allow direct visualization of agonist-

253   induced recruitment of βarr1 to a broad set of GPCRs and report βarr1 trafficking with spatio-temporal

254   resolution. Interestingly, these Intrabody sensors reveal significant conformational diversity in GPCR-

255 βarr1 complexes, which manifest in distinct contribution of βarr1 in agonist-induced ERK1/2 activation.

256 Although interaction of βarrs is highly conserved across GPCRs, there are many instances of distinct

257 functional contribution of βarrs in trafficking and signaling of different GPCRs despite having an overall

258 similar recruitment and trafficking pattern (*19*). These examples suggest that all GPCR-βarr complexes

259 formed in cells may not have identical functional abilities and recent studies have in fact started to

260 provide evidence towards this notion (*20, 21*). Intrabody sensors developed here now offer direct

261 evidence for distinct conformational signatures in βarr1, and therefore, offer important insights into the

262 process of GPCR activation, trafficking and signaling. Our data with B2R mutants also underscore that

263 βarr conformations supporting receptor endocytosis vs. ERK1/2 phosphorylation are likely to be distinct

264 from each other. This has direct implications for the conceptual framework of biased-agonism at GPCRs

265 aimed at designing novel therapeutic strategies.

275 **Author's contribution:**

276 MB and PK carried out most of the experiments related to intrabody generation, characterization,

277 confocal microscopy, co-immunoprecipitation and ERK1/2 phosphorylation; EG performed the ERK1/2

278 phosphorylation for V2R and contributed in generation of receptor mutants; SP carried out the ERK1/2

279   phosphorylation experiment together with PK; BS performed the BRET experiments under the

280   supervision of MB; SS carried out the 3-colour confocal and endosomal co-localization experiments

281   under the supervision of AH; SS measured the colocalization of V2R,βarr1 and Ib30 under the

282   supervision of AH; BS carried out the BRET experiments under the supervision of MB; AKS supervised the

283   overall project execution and management.

284   **Materials and methods**

285   **Cell Culture and Transfection**

286   HEK293 cells (ATCC) were maintained in DMEM containing 10% FBS and penicillin/streptomycin (100

287   U/mL) at 37°C in 5%CO2. Transient transfections of DNA were performed with Lipofectamine 2000 (Life

288   Technologies) and cells were assayed 48 hr post transfection. The DNAs used were: FLAG-V2R, HA-ScFv

289   control, HA-ScFv30, β-arrestin1-GFP. The antibodies used were: mouse anti-FLAG (M1, Sigma); rabbit

290   anti-HA (cell signaling); goat anti-rabbit Alexa-Fluor647 and goat anti-mouse Alexa-Fluor555 (Thermo

291   Fisher).

292   **Co-immunoprecipitation assay:** In order to screen for Fabs that selectively recognized active

293   conformation of βarr1, FLAG-tagged Receptor (3.5μg) along with βarr1 (3.5μg) in ratio 1:1 was

294   overexpressed in HEK-293 cells using PEI based transient transfection. 48h post-transfection, cells were

295   serum starved for at least 4 hrs, lysed by douncing and incubated with either Fab4,7,9 or 12 for 1h at

296   room temperature to allow a stable Receptor-βarr1-Fab complex. Subsequently, 20 μl of pre-

297   equilibrated Protein L (Capto L, GE Healthcare) beads (20mM HEPES, 150mM NaCl) was added to the

298   mixture and allowed to incubate for additional 1h. Beads were washed thrice with wash buffer

299   containing 20mM HEPES, 150mM NaCl supplemented with 0.01% MNG and eluted with 2X SDS loading

300   buffer. Eluted samples were run on 12% SDS-polyacrylamide gel electrophoresis and probed for receptor

301 using HRP-coupled anti-FLAG M2 antibody (Sigma, 1:2000). Fabs were visualized on gel using Coomassie

302 staining.

303 In order to assess the ability of intrabodies (Ib30 and Ib4) with only activated form of βarr1,

304 HEK-293 cells overexpressing FLAG-tagged Receptor (2.3µg), βarr1 (2.3µg) and HA-tagged Ibs (2.3µg)

305 were stimulated with agonist at saturated concentration 48h post-transfection. Cells were lysed in NP-

306 40 lysis buffer (Tris 50 mM; NaCl 150mM; PhosStop 1X; Protease inhibitor 1X; NP-40 1%) followed by

307 incubation with 20µl of pre-equilibrated HA beads (Sigma, A-2095) for 2h at 4°C. Beads were washed

308 thrice with wash buffer containing 20mM HEPES, 150mM NaCl maintaining cold conditions. For elution

309 2X SDS loading buffer was used. FLAG-tagged receptor was probed using HRP-coupled anti-FLAG M2

310 antibody (1:2000) while HA-tagged Ibs were detected using HA-probe antibody (sc-805, 1:5000). Ib-CTL

311 which does not recognize β-arr1 was used as a negative control in these experiments. In order to further

312 confirm that the Ib30 recognizes a functional Receptor-βarr1 complex, we overexpressed FLAG-tagged

313 β2V2R, βarr1 and HA-tagged Ib30 in HEK-293 cells. 48h post-transfection cells were stimulated with

314 agonists of varying efficacies (Inverse agonist: ICI and carazolol; partial agonists: salmeterol, salbutamol,

315 clenbuterol and norepinephrine; full agonists: Isoproterenol) and co-immunoprecipitated using HA-

316 beads agarose by the same method described above.

317 To determine the conformation of βarr1 bound to C5aR1-WT receptor versus C5aR1-V2

318 chimera, surface expression of the two receptors were first optimized by Surface ELISA and

319 subsequently transfection was carried in a way that would yield almost equal surface expression for the

320 two receptors. Accordingly, HEK-293 cells were transfected with βarr1 (3.5 µg) along with FLAG-tagged

321 C5aR1-WT (3.5 µg) or FLAG-tagged C5aR1-V2 (2.5 µg). 48 hrs post-transfection cells were starved for 4h

322 and stimulated with agonist (C5a, 100 nM). Cells were lysed by douncing and then further incubated

323 with 5 µg of Fab30 for 1h at room temperature to enable Receptor-βarr1-Fab30 complex formation.

324 Subsequently, 20 µl of pre-equilibrated Protein L (Capto L, GE Healthcare) beads (20mM HEPES, 150mM

325 NaCl) was added to the mixture and allowed to incubate for additional 1h. Beads were washed thrice

326 with wash buffer containing 20mM HEPES, 150mM NaCl supplemented with 0.01% MNG and eluted

327 with 2X SDS loading buffer. Eluted samples were run on 12% SDS-polyacrylamide gel electrophoresis and

328 probed for receptor using HRP-coupled anti-FLAG M2 antibody (Sigma, 1:2000). Fabs were visualized on

329 gel using Coomassie staining. A separate gel containing 20 µl of the whole cell lysate was run on 12% gel

330 and probed with anti-FLAG M2 antibody to compare expression of both WT and chimeric receptors.

331 In order to determine the interacting interface of the third intracellular loop (ICL3) in M2R with βarr1,

332 purified βarr1 were pre-incubated with a 10-fold molar excess of V2Rpp or alone for 30 mins at room

333 temperature. HEK-293 cell lysate overexpressing the M2R and stimulated with its agonist carbachol

334 (20µM) at 0, 5 and 15 min time points were subsequently added to the βarr1 alone or βarr1 activated

335 and saturated with V2Rpp. The reaction was allowed to proceed for 1hr at room temperature. Fab30

336 (2.5µg/reaction) was also kept in the reaction for stabilizing the M2R-βarr1 complex. Reactions with no

337 Fab30 were kept as a negative control. Following an incubation of 1 hr, pre-equilibrated M1-Flag

338 agarose beads (20uL) were added to the reaction mixture supplemented with 2mM $CaCl_2$ and incubated

339 for an additional 1h at room temperature. Beads were extensively washed twice with low salt wash

340 buffer (20mM HEPES pH 7.4, 150mM NaCl, 2mM $CaCl_2$, 0.01% MNG) first followed by washes in high salt

341 buffer (20mM HEPES pH 7.4, 150mM NaCl, 2mM $CaCl_2$, 0.01% MNG) with additional washes (twice) in

342 low salt buffer again. Bound proteins were eluted using elution buffer containing FLAG peptide (20mM

343 HEPES pH 7.4, 150mM NaCl, 2mM EDTA, 250 µg/ml FLAG peptide, 0.01% MNG,) and separated by

344 running on 12 % SDS-PAGE and visualized by Western Blotting (βarr antibody, 1:5000; anti-FLAG M2

345 antibody, 1:5000) (Figure 4C).

346

347 **Confocal microscopy.** In order to visualize the role of Ib30/Ib4 as a biosensor of GPCR activation co-

348 localization of Ibs with activated βarr1 was monitored using confocal microscopy. HEK-293 cells co-

349 transfected with Receptor (2.3μg), βarr1-m-cherry (2.3μg) and Ib-YFP (2.3μg) each. After 24 h, cells were

350 seeded on to cell culture treated confocal dishes (GenetiX; 100350) already coated with 0.01% poly-D-

351 lysine (Sigma). 48h post-transfection cells were serum starved for at least 6h prior to stimulation with

352 indicated agonists at saturating concentrations. For confocal live imaging we used Zeiss LSM 710 NLO

353 confocal microscope and samples were housed on a motorized XY stage with a CO2 enclosure and a

354 temperature controlled platform equipped with 32x array GaAsP descanned detector (Zeiss). YFP was

355 excited with a diode laser at 488 nm laser line while m-cherry was excited at 561 nm. Laser intensity and

356 pinhole settings were kept in the same range for parallel set of experiments and spectral overlap for any

357 two channels was avoided by adjusting proper filter excitation regions and bandwidths. Images were

358 scanned using the line scan mode and images were finally processed in ZEN lite (ZEN-blue/ZEN-black)

359 software suite from ZEISS. Line-scan analysis was performed using ImageJ plot profile plug-in to measure

360 fluorescence intensities across a drawn line. Graphs were plotted after intensities were normalized by

361 subtracting background.

362 **ERK1/2 MAP kinase phosphorylation assay.** For assessing the role of βarr1-mediated ERK2 activation on

363 V2R, AT1AR, B_2R, $B_2R^{\Delta G/L370T}$ and B_2R^{L370T}, HEK-293 cells with selective knockdown of βarr1, attained by

364 sh-RNA mediated transfections were used. shRNA mediated knockdown reduced the amount of βarr1

365 by ~50%. Stable selection was maintained by inclusion of G418 (1.5μg/ml) in the growth medium. About

366 3 million cells were seeded on a 10 cm cell-culture dish a day prior to transfection to achieve ~ 60%

367 confluency. For transfections, 0.5μg, 1μg and 2μg of V2R, B2R and AT1AR were used respectively. After

368 24 hrs, 1 million cells were split on to a 6 well plate. 48h post-transfection cells were serum starved for

369 at least 5 hrs in serum-free medium supplemented with 10mM HEPES (pH 7.4) and 0.1% Bovine serum

370 albumin. Cells were stimulated with an increasing dose of agonist (-log9, -log8 and –log7) and were lysed

371 using 2X SDS loading buffer, boiled at 95˚C for 15 mins.

372 In order to examine the effect of Ib30 on βarr1 mediated ERK activation, HEK-293 cells were co-

373 transfected with human Vasopressin receptor (V2R; 3.5µg) and either Ib30 or Ib-CTL (3.5µg) using PEI

374 based transient transfection. After 24h, one million cells were plated on a six-well plate. 48h post-

375 transfection cells were serum starved for at least 4h and stimulated with agonist (AVP,100 nM).

376 Following stimulation cells were lysed using 2X SDS loading buffer, boiled at 95˚C for 15 mins and loaded

377 onto 12% SDS-polyacrylamide gel electrophoresis. All experiments were carried out on HEK-293 cells

378 with low passage and maintained in Dulbecco's modified Eagle's complete media (Sigma) supplemented

379 with 10% fetal bovine serum (Thermo Scientific) and 1% penicillin–streptomycin at 37℃ under 5% CO_2.

380 For detecting phosphorylation of ERK1/2 in both HEK-293 cells and knockdown cells Western

381 blotting analysis of the whole-cell lysate was performed and transferred to polyvinylidene difluoride

382 membranes (PVDF;BioRad).The membrane was blocked with 5% BSA (SRL) for 1℃h and then probed with

383 anti-pERK primary antibody (CST, catalog number. 9101; 1:5,000 dilution) overnight at 4℃°C followed by

384 1℃h incubation with anti-rabbit IgG secondary antibody (Genscript, catalog number. A00098) at room

385 temperature. The membrane was then washed with 1 × TBST thrice and developed using Chemi Doc

386 (BioRad). The anti-pERK antibody was stripped-off using 1X stripping buffer and then reprobed with anti-

387 tERK antibody (CST, catalog number. 9102 and 4695; 1:5,000 dilution).

388 **Three-channel confocal Imaging Imaging**

389 Receptor imaging of live or fixed cells was monitored by ''feeding'' cells with Alexa-Fluor555-conjugated

390 FLAG antibody (15 min, 37°C) in phenol-red-free DMEM prior to agonist treatment. Fixed cells were

391 washed three times in PBS/0.04% EDTA to remove FLAG antibody bound to the remaining surface

392 receptors, fixed using 4% PFA (20 min at RT), permeabilized and stained using HA primary antibody

17

393   followed by Alexa-Fluor647 secondary antibody. For co-localization of FLAG-V2R with endosomal

394   markers, cells were treated as above except incubated with either of the following primary antibodies

395   post-permeabilization; EEA1 (rabbit anti-EEA1 antibody from Cell Signaling Technology) or APPL1 (rabbit

396   anti-APPL1 antibody from Cell Signaling Technology). Cells were imaged using a TCS-SP5 confocal

397   microscope (Leica) with a 63x 1.4 numerical aperture (NA) objective and solid-state lasers of 488 nm,

398   561 nm, and/or 642 nm as light sources. Leica LAS AF image acquisition software was utilized. All

399   subsequent raw-image tiff files were analyzed using ImageJ or LAS AF Lite (Leica).

400   **GloSensor Assay.** To assess the role of Ib30 on G protein signalling and desensitization GloSensor assay

401   was performed with only vasopressin receptor system. HEK-293 cells were triple transfected with

402   human Vasopressin receptor (V2R receptor; 2.3µg), the luciferase-based cAMP biosensor (2.3 µg;

403   pGloSensorTM-22F plasmid; Promega) and Ib30/Ib-CTL (2.3 µg) using PEI based transient transfections.

404   14–16 h post-transfection, media was aspirated and cells were flushed and pooled together in assay

405   buffer containing 1X Hanks balanced salt solution, pH 7.4 and 20 mM of 4-(2-hydroxyethyl)-1-

406   piperazineethanesulfonic acid [HEPES]. Density of the cells was determined by counting on

407   haemocytometer and subsequently the volume of cells that should yield 125,000 cells per 100µl in a 96

408   well plate was calculated. Cells were pelleted at 2000 rpm for 3 mins to remove the assay buffer and the

409   pellet was resuspended in the desired volume of sodium luciferin solution prepared in the same assay

410   buffer. After seeding the cells in a 96 well plate it was allowed to incubate at 37°C for 90 min followed

411   by an additional incubation of 30 mins at room temperature. For stimulation various doses of ligand

412   (AVP) were prepared by serial dilution ranging from 0.1 pM to 1 µM and added to the cells with help of a

413   multichannel pipette. Luminescence was recorded using a microplate reader (Victor X4; Perkin Elmer).

414   Effect of Ib30 was compared to Ib-CTL and normalized with respect to maximal stimulation by agonist

415   (treated as 100%). Data were plotted and analyzed using nonlinear regression in GraphPad Prism

416   software.

417 **BRET assay**

418 Transient transfections were performed on cells seeded (40,000 cells/100 µl/well) in white 96-well

419 microplates (Greiner) using 25 kDa linear polyethylenimine (PEI) as transfecting agent, at a ratio of 4:1

420 PEI/DNA. To monitor receptor or β-arrestin trafficking from the cell surface or in the endosomes, we

421 used enhanced bystander BRET (ebBRET) where the BRET acceptor, a *Renilla* green fluorescent protein

422 (rGFP), is fused to either CAAX or FYVE domains from Kras and endofin proteins respectively to target

423 respectively the plasma membrane (rGFP-CAAX) or the early endosomes (rGFP-FYVE); the receptor or β-

424 arrestin are fused to the BRET donor *Renilla* luciferase II (RlucII) (*22*). To monitor β-arrestin interaction

425 with V2R, we used β-arrestin fused to RlucII and V2R fused to the yellow variant of the *aquaria Victoria*

426 green fluorescent protein, YFP (*23*). Forty-eight hours later, culture media was removed, cells were

427 washed with DPBS (Dulbecco's Phosphate Buffered Saline) and replaced by HBSS (Hank's Balanced Salt

428 Solution). For time-course experiment, after a 3 minutes pre-incubation with of 2.5 µM coelenterazine H

429 (BRET1 for V2R β-arrestin interaction) from Goldbio or coelenterazine 400a (BRET2 for CAAX and FYVE

430 assays) from Nanolight Technology, cells were stimulated with vehicle or AVP (100 nM) and BRET was

431 measured every 45 seconds for 20 minutes. For concentration-response curves, cells were stimulated

432 with increasing concentrations of AVP for 10 minutes and 2.5µM coelenterazine H (BRET1) or

433 coelenterazine 400a (BRET2) was added 5 minutes before BRET measurement. BRET signals were

434 recorded on a Mithras (Berthold scientific) microplate reader equipped with the following filters:

435 480/20 nm (donor) and 530/20 nm (acceptor) for BRET1 or 400/70 nm (donor) and 515/20 nm

436 (acceptor) for BRET2. The BRET signal was determined as the ratio of the light emitted by the energy

437 acceptor over the light emitted by energy donor. The agonist-promoted BRET signal (ΔBRET) was

438 obtained by subtracting the BRET signal recorded in the presence of vehicle from that obtained

439 following AVP treatment.

440   **Receptor and intrabody expression**

441   To assess the receptor and intrabodies expression levels, we took advantage of the FLAG epitope fused

442   at the N-terminus of the V2R (FLAG-V2R) and a HA epitope tag fused at the C-terminus of the

443   intrabodies. Their relative expression was monitored by ELISA using anti-FLAG-HRP (Sigma) or anti-HA-

444   HRP antibodies (Roche Diagnostics). Cells were fixed with 3% formaldehyde for 10 min and

445   permeabilized with 0.1% triton X-100 to monitor the intrabodies expression. Cells were washed three

446   times in washing buffer (1% BSA in DPBS), followed by a blocking step by incubating the cells for 1 hour

447   in washing buffer. The horse radish peroxidase-conjugated antibody was then added for 1h at room

448   temperature and the HRP activity was measured by adding o-phenylenediamine dihydrochloride

449   (Sigma–Aldrich). The reaction was stopped by adding 0.6 M HCl followed by absorbance measurement

450   at 492nm using a SpectraMax 190 plate reader (Molecular Devices).

451   **Molecular Dynamics simulation**

452   In order to generate the complexes of the B2Rpp WT, the L370pT mutant of B2Rpp and the V2Rpp

453   bound to βarr1, we used the structure of V2Rpp in complex with βarr1 (PDB code: 4JQI). Missing

454   fragments in the βarr1 and V2Rpp structures were modelled using the loop modeler module available in

455   the MOE package (https://www.chemcomp.com). B2Rpp and B2Rpp mutant systems were obtained by

456   converting the sequence of the V2Rpp into that of the B2Rpp and the corresponding L370pT mutant.

457   Finally, the co-crystallized FAB30 antibody was removed.

458   The complexes were solvated in TIP3P water, with the ionic strength kept at 0.15 M using NaCl

459   ions. Simulation parameters were obtained from the Charmm36M forcefield1. Systems generated this

460   way were simulated using the ACEMD software package2. To allow rearrangement of waters and

461   sidechains, we carried out a 25ns equilibration phase in NPT conditions with restraints applied to

462   backbone atoms. The timestep was set to 2 fs and the pressure was kept constant, using the Berendsen

463   barostat. After the equilibration, systems were simulated in NVT conditions for 1µs in 4 parallel runs

464   employing a 4fs timestep. For all runs temperature was kept at 300 K using the Langevin thermostat and

465   hydrogen bonds were restrained using the RATTLE algorithm. Non-bonded interactions were cut-off at 9

466   Å with a smooth switching function applied at 7.5 Å. Before carrying out the structural analysis,

467   simulation frames were aligned using the backbone atoms of the βarr1. To assess the magnitude of salt

468   bridge formation between phosphorylated threonines (pT) residues and K294, we quantified frames in

469   which the protonated nitrogen of K294 and oxygens of the phosphate group of each respective pT

470   adopted a distance of 3.2 Å or less. Conformational variability of the lariat loop was studied with the

471   clustering tool available in VMD3. As a clustering parameter we used RMSD (cutoff: 2.2) of the backbone

472   atoms of residues 293 to 297 within the lariat loop.

473   **Figure legends.**

474   **Figure 1. Generation and characterization of intrabody sensors for βarr1 recruitment and trafficking.**

475   **A.** Schematic representation of conversion of Fabs into ScFv format for intracellular expression (i.e.

476   intrabodies). **B.** Expression analysis of intrabodies in HEK-293 cells as visualized by Western blotting.

477   Lysate prepared from HEK-293 cells expressing the indicated intrabodies were separated on SDS-PAGE

478   followed by visualization using anti-HA antibody. **C.** Cytoplasmic distribution of selected intrabodies as

479   visualized by confocal microscopy. HEK-293 cells expressing βarr1-mCherry and YFP-tagged intrabodies

480   were subjected to live cell imaging which revealed even distribution of intrabodies in the cytoplasm and

481   nuclear localization. Scale bar is 10µm. **D.** Ability of intrabodies to recognize receptor-bound βarr1. HEK-

482   293 cells expressing β2V2R, βarr1 and intrabodies were stimulated with either an inverse-agonist

483   (carazolol) or agonist (Isoproterenol) followed by co-immunoprecipitation using anti-HA antibody

484   agarose. The proteins were visualized by Western blotting using anti-Flag M2 antibody and anti-HA

485   antibody. The bottom panel shows densitometry-based quantification of the data (average±SEM) from

486 three independent experiments. **F.** The ability of Intrabody30 (Ib30) to recognize receptor-βarr1

487 complex mirrors the ligand efficacy. HEK-293 cells expressing β2V2R, βarr1 and intrabodies were

488 stimulated with indicated ligands followed by co-IP and Western blotting as mentioned above. **G.**

489 Densitometry-based quantification of the data (average±SEM) from three independent experiments. For

490 isoproterenol, which yields maximal signal, only 10% of the total elution is loaded to avoid signal

491 saturation. **H.** Intrabody30 reports agonist-induced βarr1 trafficking. HEK-293 cells expressing β2V2R,

492 βarr1-mCherry and Ib30-YFP were stimulated with agonist (isoproterenol) for indicated time-points and

493 the localization of βarr1 and Ib30 were visualized using confocal microscopy. Scale bar is 10 μm.

494 **Figure 2. Intrabody30 as a generic sensor of βarr1 recruitment and trafficking for a set of chimeric**

495 **GPCRs.** HEK-293 cells expressing βarr1 (or βarr1-mCherry) and Ib30 (HA or GFP-tagged) were co-

496 transfected with plasmids encoding N-terminally-FLAG tagged α2BV2R (**A**), CCR2V2R (**B**), D2V2R (**C**),

497 D5V2R (**D**), M5V2R (**E**) and C5aR1V2R (**F**). Subsequently, cells were stimulated with respective agonists

498 followed by co-immunoprecipitation using anti-HA antibody agarose. The proteins were visualized by

499 Western blotting using anti-Flag M2 antibody and Simply Blue protein staining reagent (CBB) (Left

500 panels). The right panels show the ability of Ib30 to report agonist-induced βarr1 trafficking for the

501 corresponding GPCRs. HEK-293 cells expressing the respective receptor, βarr1-mCherry and Ib30-YFP

502 were stimulated with agonist for indicated time-points and the localization of βarr1 and Ib30 were

503 visualized using confocal microscopy (middle panels). Scale bar is 10μm. Right panels show line-scan

504 analysis of images presented in the third sub-panel of confocal micrographs to demonstrate

505 colocalization of βarr1-mCherry and IB30-YFP. Densitometry-based quantification of coIP data presented

506 above (in panels B, F, J, N, R, V A – F) from three independent experiments normalized with respect to

507 maximum signal for each receptor system (treated as 100%), and analyzed using One-way-ANOVA.

508 **Figure 3. Intrabody30 sensor reveals conformational differences in βarr1 recruited to different class B**

509 **GPCRs. A.** G-protein-coupling preference and phospho-codes in a set of class B GPCRs (with respect to

510 βarr recruitment pattern). Complete phospho-codes in these receptors are identified based on a recent

511 study (17). **B.** Ib30-YFP sensor reports the recruitment and trafficking of βarr1 for several class B GPCRs

512 such as V2R, C5aR1, ACKR2 and M2R, it does not recognize βarr1 upon activation of other class B GPCRs

513 such as AT1aR and B2R as presented in panel **C.** For these experiments, HEK-293 cells expressing native

514 GPCRs (as indicated in the respective panels), βarr1-mCherry and Ib30-YFP were stimulated with

515 respective agonists for indicated time-points, and the localization of βarr1 and Ib30 were visualized

516 using confocal microscopy. Scale bar is 10μm. **D.** The ability of Ib30 to recognize receptor-bound βarr1 is

517 further confirmed by co-immunoprecipitation experiment. HEK-293 cells expressing either V2R or

518 C5aR1, βarr1 and HA-tagged Ib30 were stimulated with agonist (100nM followed by co-

519 immunoprecipitation using anti-HA antibody agarose. The proteins were visualized by Western blotting

520 using anti-Flag M2 antibody and anti-HA antibody. The bottom panel shows densitometry-based

521 quantification of the data (average±SEM) from three independent experiments normalized with respect

522 to maximum reactivity (treated as 100%). Data are analyzed using One-Way-Anova with Bonferroni post-

523 test (*p <0.05; ***p <0.001).

524 **Figure 4. Intrabody30 sensor reveals conformational differences in βarr1 recruited to different class A**

525 **GPCRs. A.** G-protein-coupling preference and phospho-codes in a set of class A GPCRs (with respect to

526 βarr recruitment pattern). Complete phospho-codes in these receptors are identified based on a recent

527 study (17). **B.** Ib30-YFP sensor reports the recruitment and trafficking of βarr1 for M3R and M5R but it

528 does not recognize βarr1 upon activation of other class A GPCRs such as β2AR and D2R. α2BR does not

529 exhibit agonist-induced βarr1 recruitment despite having three potential phosphorylation codes in the

530 3rd intracellular loops. For these experiments, HEK-293 cells expressing native GPCRs (as indicated in the

531 respective panels), βarr1-mCherry and Ib30-YFP were stimulated with respective agonists for indicated

23

532   time-points, and the localization of βarr1 and Ib30 were visualized using confocal microscopy. Scale bar

533   is 10μm. **C.** The interaction of M2R with βarr1 is inhibited by V2Rpp suggesting an overlapping docking

534   interface of its ICL3 with that of V2Rpp. The upper panel displays schematic representation of the V2R

535   and M2R to underline the presence of phosphorylation sites (shown in red) in the carboxyl-terminus and

536   ICL3, respectively. HEK-293 cells expressing M2R were stimulated with agonist followed by addition of

537   purified βarr1 (with or without pre-incubation of V2Rpp) and Fab30. Subsequently, the receptor is co-

538   immunoprecipitated using anti-Flag M1 agarose beads and proteins were visualized by Western blotting

539   using anti-Flag M2 antibody and anti-βarr1 antibody. The bottom panel shows densitometry-based

540   quantification of the data (average±SEM) from two independent experiments normalized with respect

541   to maximum reactivity (treated as 100%). Data are analyzed using One-Way-Anova with Bonferroni post-

542   test (**p <0.01).

543   **Figure 5. Distinct conformations of receptor-bound βarr1 are linked with different functional**

544   **outcomes.** Different conformations of receptor-bound βarr1 drive their distinct functional contribution

545   in agonist-induced ERK1/2 MAP kinase phosphorylation for V2R and B2R. Agonist-induced

546   phosphorylation of ERK1/2 in HEK-293 cells expressing either V2R (**A**) or B2R (**B**) in presence and

547   absence of βarr1 knock-down are measured using Western blotting. Densitometry-based quantification

548   of data from three independent experiments is presented as bar-graphs in the right panels normalized

549   with respect to maximal signal under control condition (treated as 100%) and analyzed using One-way-

550   ANOVA with Bonferroni post-test (**p <0.01). **C.** Comparison of spatial distribution of phosphorylation

551   sites in V2R and B2R. The double mutant of B2R, referred to as B2R$^{\Delta G/L370T}$, is generated to mimic the

552   spatial distribution of Ser/Thr in V2R. Confocal microscopy reveals robust recognition of βarr1 upon

553   agonist-stimulation of B2R$^{\Delta G/L370T}$. HEK-293 cells expressing B2R$^{\Delta G/L370T}$, βarr1-mCherry and Ib30-YFP were

554   stimulated with agonist (bradykinin, 1μM) for indicated time-points and the localization of βarr1 and

555   Ib30 were visualized using confocal microscopy. Scale bar is 10μm. **D.** Knock-down of βarr1 robustly

556   inhibits agonist-induced ERK1/2 phosphorylation for B2R$^{\Delta G/L370T}$, similar to V2R and in stark contrast with

557   wild-type B2R. HEK-293 cells expressing B2R$^{\Delta G/L370T}$ in presence and absence of βarr1 knock-down were

558   stimulated with indicated doses of bradykinin for 10 min followed by detection of phosphorylated

559   ERK1/2 using Western blotting. Densitometry-based quantification of data from three independent

560   experiments is presented as bar-graphs in the lower panel normalized with respect to maximal signal

561   under control condition (treated as 100%) and analyzed using One-way-ANOVA with Bonferroni post-

562   test ($*p < 0.05$; $**p < 0.01$).

563

564

565

566

567

568

569

570

571

572

573

574

575 **References**

576   1.   Y. K. Peterson, L. M. Luttrell, The Diverse Roles of Arrestin Scaffolds in G Protein-Coupled
577   Receptor Signaling. *Pharmacol Rev* **69**, 256-297 (2017).
578   2.   R. Irannejad *et al.*, Conformational biosensors reveal GPCR signalling from endosomes. *Nature*
579   **495**, 534-538 (2013).
580   3.   D. S. Kang, X. Tian, J. L. Benovic, Role of beta-arrestins and arrestin domain-containing proteins
581   in G protein-coupled receptor trafficking. *Curr Opin Cell Biol* **27**, 63-71 (2014).
582   4.   R. Ranjan, H. Dwivedi, M. Baidya, M. Kumar, A. K. Shukla, Novel Structural Insights into GPCR-
583   beta-Arrestin Interaction and Signaling. *Trends Cell Biol* **27**, 851-862 (2017).
584   5.   S. K. Shenoy, R. J. Lefkowitz, beta-Arrestin-mediated receptor trafficking and signal transduction.
585   *Trends Pharmacol Sci* **32**, 521-533 (2011).
586   6.   R. H. Oakley, S. A. Laporte, J. A. Holt, M. G. Caron, L. S. Barak, Differential affinities of visual
587   arrestin, beta arrestin1, and beta arrestin2 for G protein-coupled receptors delineate two major
588   classes of receptors. *J Biol Chem* **275**, 17201-17210 (2000).
589   7.   S. M. DeWire, S. Ahn, R. J. Lefkowitz, S. K. Shenoy, Beta-arrestins and cell signaling. *Annu Rev
590   Physiol* **69**, 483-510 (2007).
591   8.   R. S. Haider, A. Godbole, C. Hoffmann, To sense or not to sense-new insights from GPCR-based
592   and arrestin-based biosensors. *Curr Opin Cell Biol* **57**, 16-24 (2018).
593   9.   D. L. Bassoni, W. J. Raab, P. L. Achacoso, C. Y. Loh, T. S. Wehrman, Measurements of beta-
594   arrestin recruitment to activated seven transmembrane receptors using enzyme
595   complementation. *Methods Mol Biol* **897**, 181-203 (2012).
596   10. G. Barnea *et al.*, The genetic design of signaling cascades to record receptor activation. *Proc Natl
597   Acad Sci U S A* **105**, 64-69 (2008).
598   11. V. V. Gurevich, E. V. Gurevich, The molecular acrobatics of arrestin activation. *Trends Pharmacol
599   Sci* **25**, 105-111 (2004).
600   12. K. Xiao, S. K. Shenoy, K. Nobles, R. J. Lefkowitz, Activation-dependent conformational changes in
601   {beta}-arrestin 2. *J Biol Chem* **279**, 55744-55753 (2004).
602   13. K. N. Nobles, Z. Guan, K. Xiao, T. G. Oas, R. J. Lefkowitz, The active conformation of beta-
603   arrestin1: direct evidence for the phosphate sensor in the N-domain and conformational
604   differences in the active states of beta-arrestins1 and -2. *J Biol Chem* **282**, 21370-21381 (2007).
605   14. A. K. Shukla *et al.*, Structure of active beta-arrestin-1 bound to a G-protein-coupled receptor
606   phosphopeptide. *Nature* **497**, 137-141 (2013).
607   15. E. Ghosh *et al.*, A synthetic intrabody-based selective and generic inhibitor of GPCR endocytosis.
608   *Nat Nanotechnol* **12**, 1190-1198 (2017).
609   16. A. K. Shukla *et al.*, Visualization of arrestin recruitment by a G-protein-coupled receptor. *Nature*
610   **512**, 218-222 (2014).
611   17. X. E. Zhou *et al.*, Identification of Phosphorylation Codes for Arrestin Recruitment by G Protein-
612   Coupled Receptors. *Cell* **170**, 457-469 e413 (2017).
613   18. S. R. Jung, C. Kushmerick, J. B. Seo, D. S. Koh, B. Hille, Muscarinic receptor regulates extracellular
614   signal regulated kinase by two modes of arrestin binding. *Proc Natl Acad Sci U S A* **114**, E5579-
615   E5588 (2017).
616   19. S. Ahn, H. Wei, T. R. Garrison, R. J. Lefkowitz, Reciprocal regulation of angiotensin receptor-
617   activated extracellular signal-regulated kinases by beta-arrestins 1 and 2. *J Biol Chem* **279**, 7807-
618   7811 (2004).
619   20. M. H. Lee *et al.*, The conformational signature of beta-arrestin2 predicts its trafficking and
620   signalling functions. *Nature* **531**, 665-668 (2016).

621 21. S. Nuber *et al.*, beta-Arrestin biosensors reveal a rapid, receptor-dependent
622   activation/deactivation cycle. *Nature* **531**, 661-664 (2016).
623 22. Y. Namkung *et al.*, Monitoring G protein-coupled receptor and β-arrestin trafficking in live cells
624   using enhanced bystander BRET. *Nature Communications* **7**, 12178 (2016).
625 23. M. D. Rochdi *et al.*, Functional Characterization of Vasopressin Type 2 Receptor Substitutions
626   (R137H/C/L) Leading to Nephrogenic Diabetes Insipidus and Nephrogenic Syndrome of
627   Inappropriate Antidiuresis: Implications for Treatments. *Molecular Pharmacology* **77**, 836-845
628   (2010).

629

Figure 1.
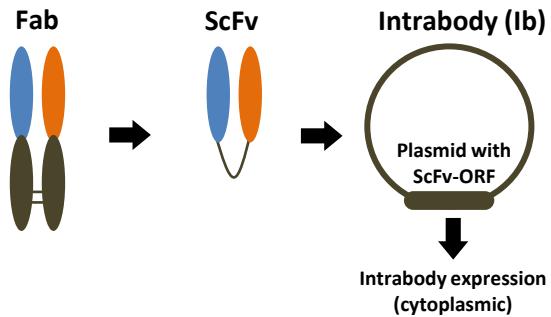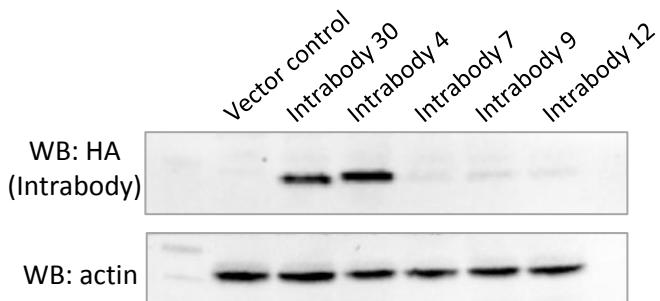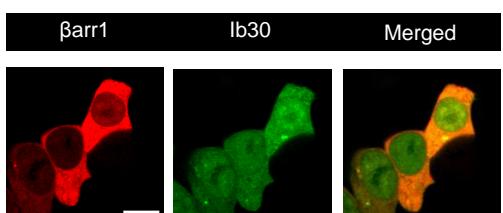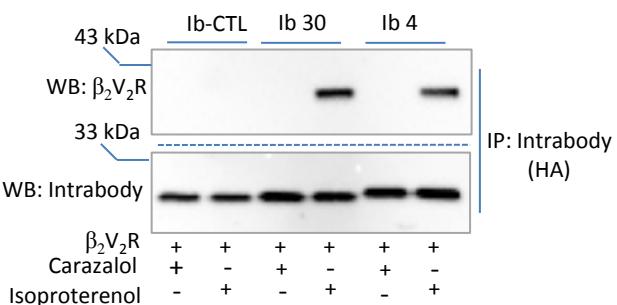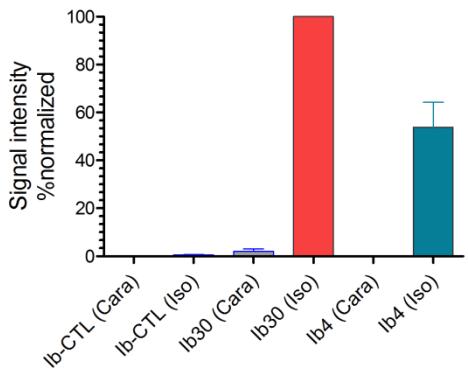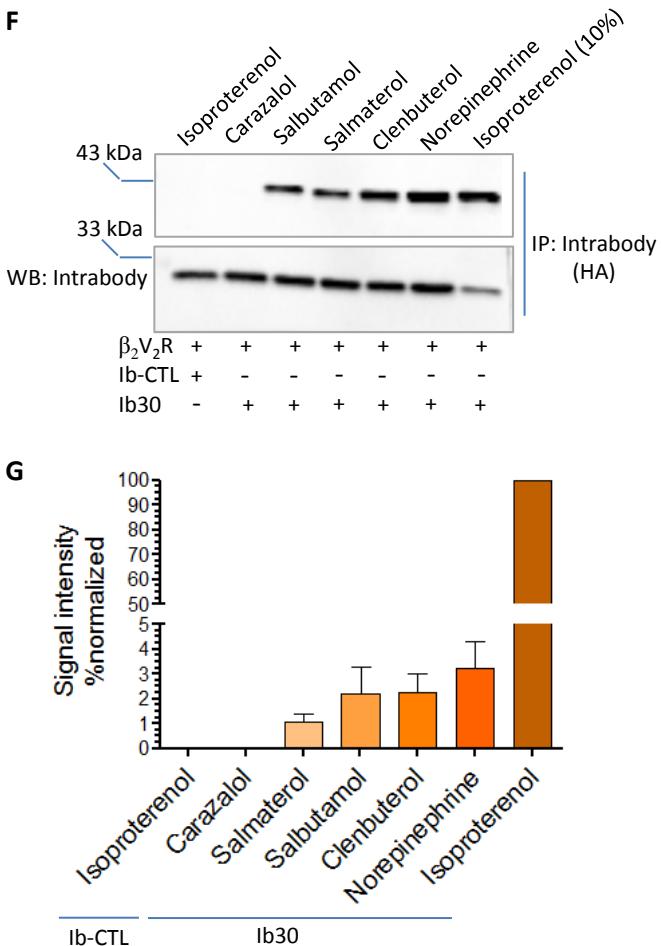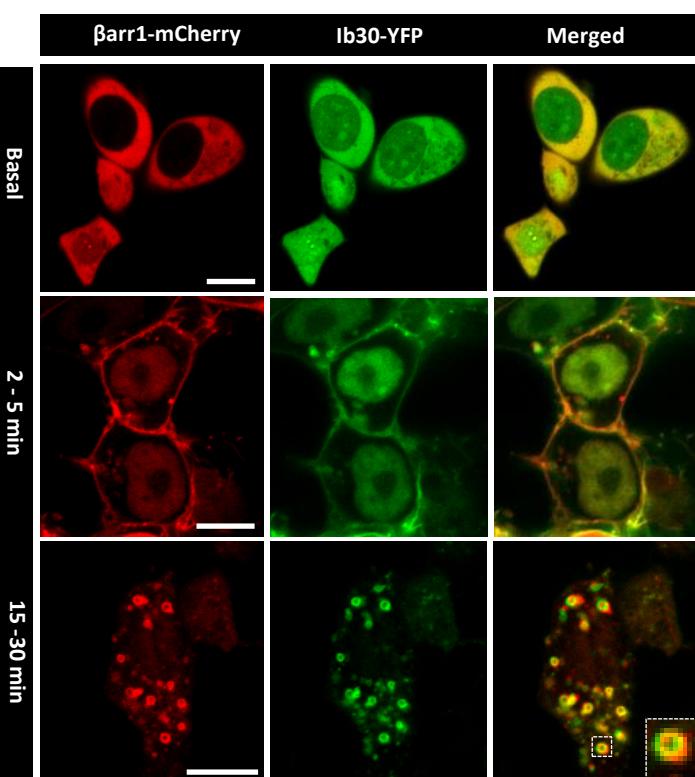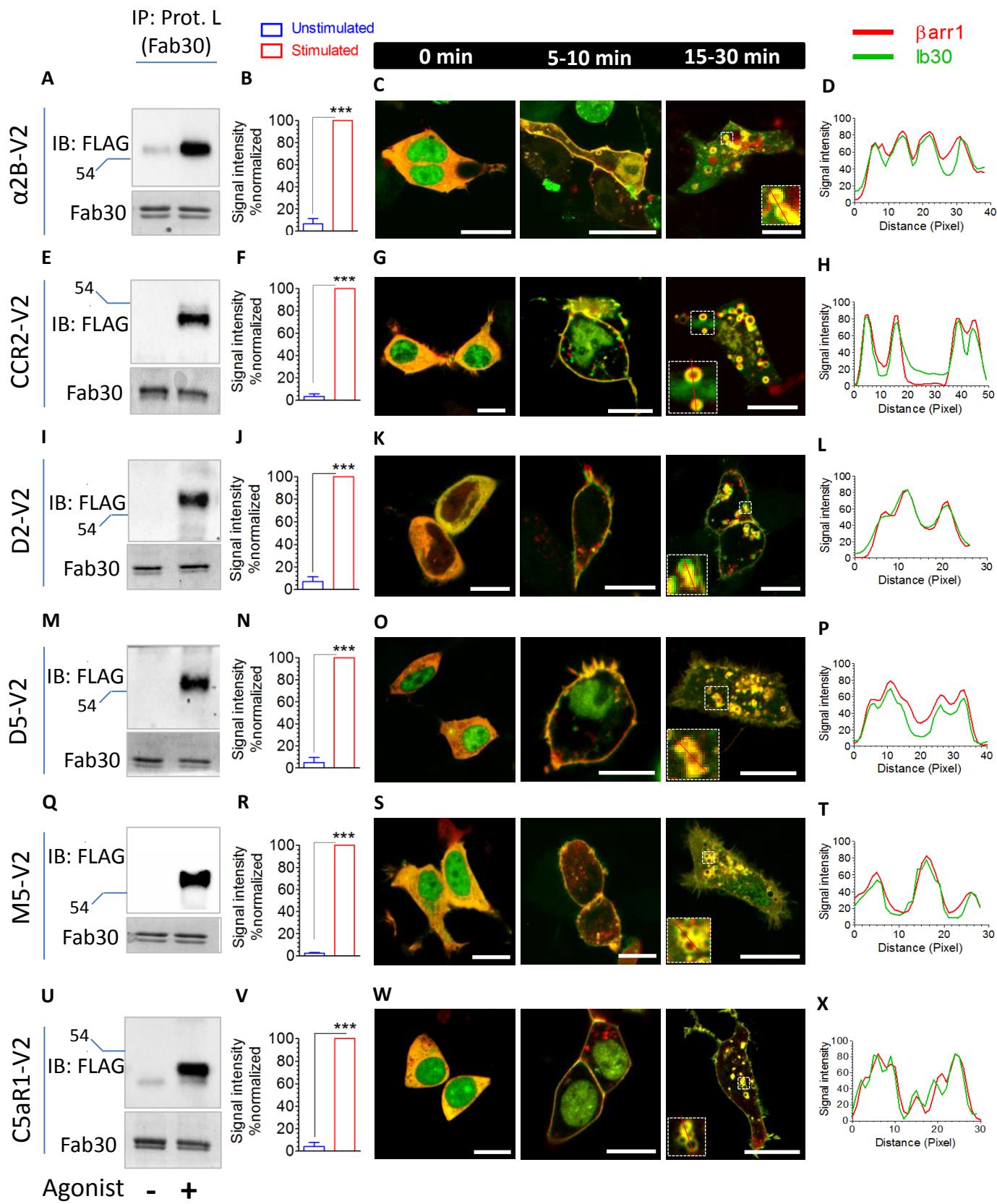
Figure 2.

Figure 3.

A

Receptor	Class A/B	G-protein	Phospho-code
V_2R	Class B	Gαs	[02] [C-term] [^{357}SCTTAS^{362}] [^{357}SCTTASS^{363}]
B_2R	Class B	Gαq	[02] [C-term] [^{325}SMGTLRT^{331}] [^{328}TLRTSIS^{334}]
$AT_{1a}R$	Class B	Gαq	[02] [C-term] [^{326}SHSNLS^{331}] [^{332}TKMSTLS^{338}]
M2R	Class B	Gαi	[02] [ICL3] [^{338}TPTNTT^{343}] [^{340}TNTTVE^{345}]
C5aR1	Class B	Gαi	[03] [C-term] [^{319}SFTRST^{324}][^{321}TRSTVD^{326}][^{321}TRSTVDT^{327}]
ACKR2	Class B	None	[06] [C-term][^{343}SLSSCS^{348}] [^{343}SLSSCSE^{349}] [^{345}SSCSESS^{352}] [^{346}SCSESS^{351}][^{348}SESSILT^{354}] [^{351}SILTAQE^{357}]
$V_{1B}R$	Class B	Gαq	[03] [C-term][^{368}SDGSLSS^{374}][^{371}SLSSRHT^{377}] [^{378}TLLTRSS^{384}]

B

βarr1-mCherry	Ib30-YFP	Merged

V_2R (5 -10 min)

V_2R (15 -30 min)

C5aR1 (15 -30 min)

M2R (15 -30 min)

ACKR2 (15 -30 min)

$V_{1B}R$ (15 -30 min)

C

βarr1-mCherry	Ib30-YFP	Merged

AT1aR (15 -30 min)

B2R (5 - 10 min)

B2R (15 -30 min)

D

IP: HA (Ib30)

AVP (min)   0   30

IB: FLAG (GPCR) — 54

WB: HA (Ib) — 29

IP: HA (Ib30)

C5a (min)   0   5   15

IB: FLAG (GPCR) — 54

WB: HA (Ib) — 29

Signal intensity %normalized

0 min   30 min   ***

Signal intensity %normalized

0 min   5 min   15 min   *   ***
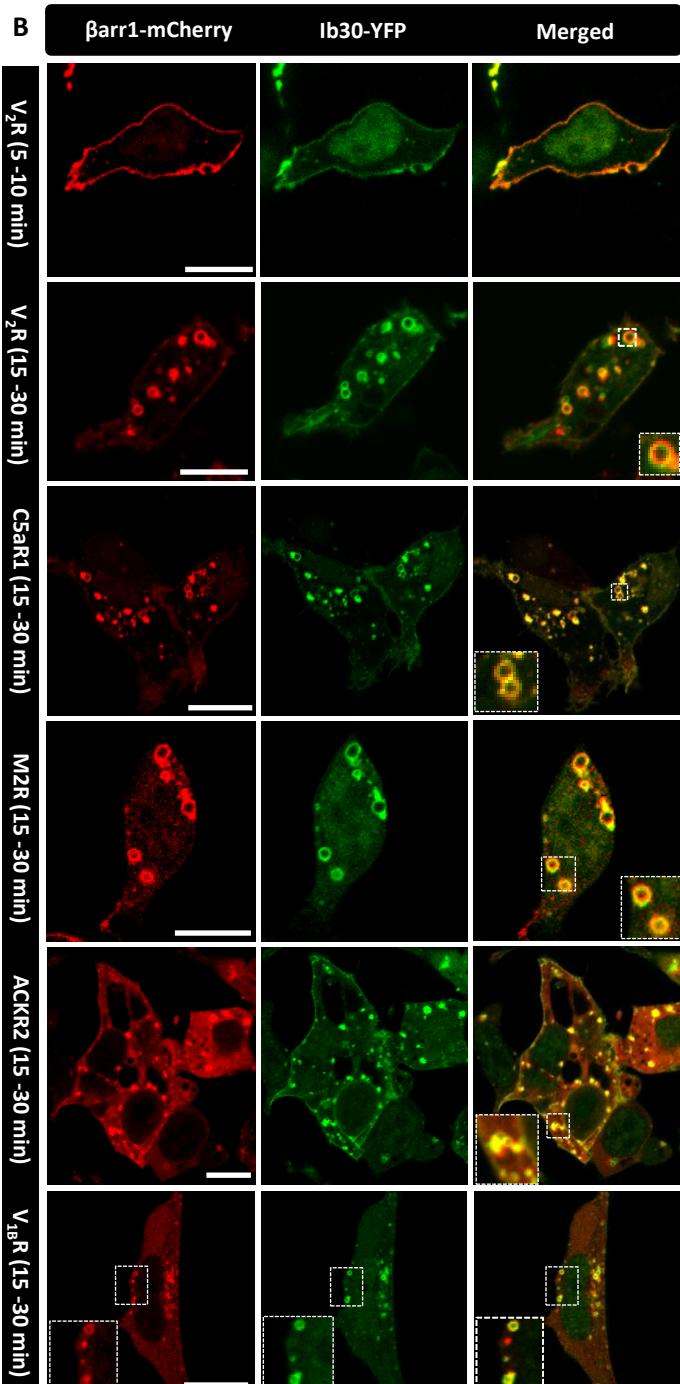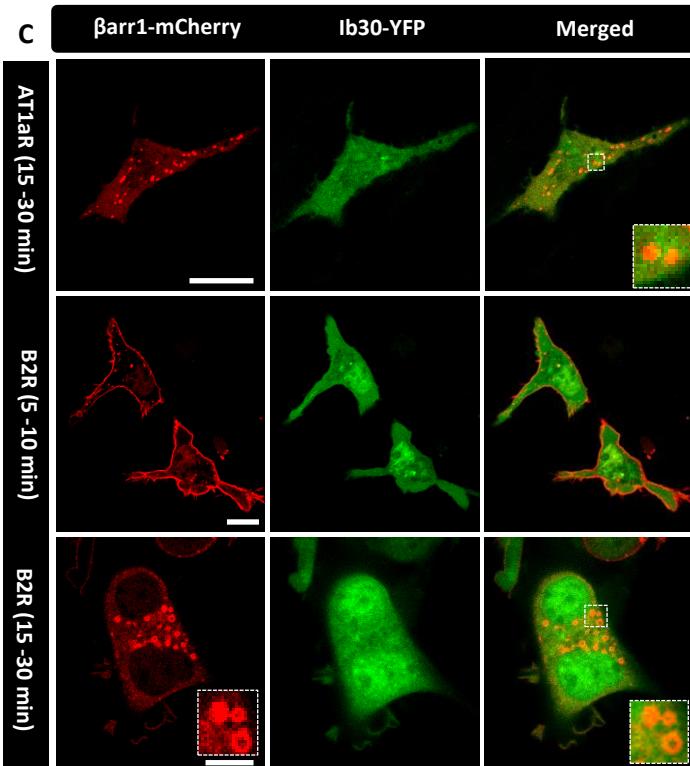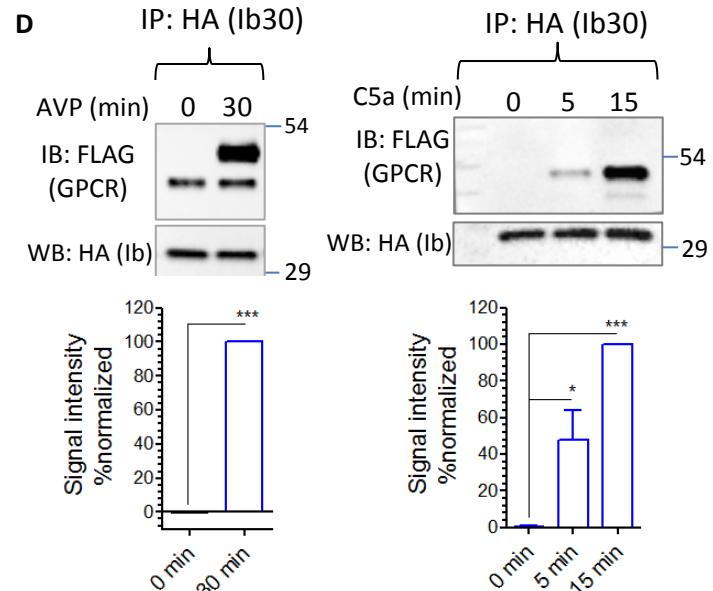
Figure 4.

Receptor	Class A/B	G-protein	Phospho-code
β_2AR	Class A	Gαs	None
D_2R	Class A	Gαi	[01] [ICL3] [^{351}TRTSLKT^{357}]
α2BR	Class A	Gαi	[03] [ICL3] [^{239}SVASARE^{245}] [^{250}SKSTGE^{255}] [^{315}SPASACS^{321}]
M_3R	Class A	Gαq	[08]] [ICL3] [^{271}SGTEAE^{276}] [^{283}TGSSRS^{289}] [^{286}SSRSCSS^{292}] [^{287}SRSCSS^{292}] [^{289}SCSSYE^{294}] [^{349}SASSDE^{354}] [^{349}SASSDEE^{355}] [^{371}TRSQIT^{376}]
M_5R	Class A	Gαq	[03]] [ICL3] [^{235}SVTKAE^{240}] [^{272}SSSRRS^{277}] [^{274}SRRSTST^{280}]

B

| βarr1-mCherry | Ib30-YFP | Merged |

M3R (15 -30 min)

M5R (15 -30 min)

D2R (5 -15 min)

β₂AR (5 -15 min)

α₂BR (15 -30 min)

C

V2R   M2R

Long C tail & Short ICL3

Short C tail & Long ICL3

Signal intensity %normalized

IB: βarr — 71 / 54

IB: FLAG (M2R) — 71 / 54

IP: FLAG (Receptor)

| Stim Time (min) | 0 | 5 | 15 | 0 | 5 | 15 |
| V2Rpp | - | - | - | + | + | + |

Fab30

Figure 5.

A

V$_2$R

CTL   βarr1-KD

0 1 10 100   0 1 10 100   AVP (nM)

pERK

tERK

□ CTL
□ βarr1-KD

*** ***

pERK/tERK (%normalized)

120
100
80
60
40
20
0

-8   -7
AVP -log [M]

B

B2R

CTL   βarr1-KD

0 1 10 100   0 1 10 100   Brady (nM)

pERK

tERK

□ CTL
□ βarr1-KD

** **

pERK/tERK (%normalized)

350
300
250
200
150
100
50
0

-8   -7
Brady -log [M]

C

V$_2$R   SC TT A SSSL
B$_2$R   SMG TL R TSIS
B$_2$R$^{\Delta G/L370T}$ SM TT R TSIS

βarr1-mCherry	Ib30-YFP	Merged

Basal

2 - 5 min

15 -30 min

D

B$_2$R$^{\Delta G/L370T}$

CTL   βarr1-KD

0 1 10 100   0 1 10 100   Brady (nM)

pERK

tERK

□ CTL
□ βarr1-KD

*   **

pERK/TERK (%normalized)

120
100
80
60
40
20
0

0   -9   -8   -7
Brady -log [M]